

# Gravitational Waves from Phase Transitions

Djuna Lize Croon\*      David James Weir†

October 30, 2024

## Abstract

We summarise the physics of first-order phase transitions in the early universe, and the possible ways in which they might come about. We then focus on gravitational waves, emphasising general qualitative features of stochastic backgrounds produced by early universe phase transitions and the cosmology of their present-day appearance. Finally, we conclude by discussing some of the ways in which a stochastic background might be detected.

## 1 Introduction

Our understanding of the history of our universe has improved dramatically over the past two decades. Three generations of space probes have mapped out the electromagnetic echoes of the Big Bang – the cosmic microwave background radiation – to unprecedented precision [1]. Experiments at the Large Hadron Collider (LHC) finally discovered the Higgs boson [2, 3], cementing a keystone of the so-called Standard Model (SM) of particle physics. In recent years, we have also been able to directly detect gravitational waves from merging black holes [4] and neutron stars [5]. Each of these discoveries is another milestone in our quest to understand where we come from. Furthermore, each discovery represents a different facet of modern physics: early universe cosmology, experimental particle physics, and gravitational wave astrophysics.

Indeed, the earliest seconds of our universe have been the topic of speculation and scientific inquiry since the earliest civilisations. At present, we have a reasonably good understanding of the different stages that must have occurred, but important open questions remain to be answered. The aim of this present work is to show how the three facets mentioned above, in which so much recent progress has been made, might help us understand the universe’s very earliest moments.

As the universe expanded and cooled down, it is likely to have gone through one or more phase transitions. In this context, a phase transition is a cosmological processes in which the bulk properties of the very early universe changed considerably over a relatively short time. They are analogous to the changes of phase seen in water in everyday life: as it cools, water vapour condenses and then freezes (see Fig. 1) – three phases with very different bulk properties. In the early universe these phase transitions leave signatures which, if detected, could help to explain some of the mysteries that still persist, such as the imbalance between matter and antimatter in the present universe: the observable universe is overwhelmingly made of matter, and we are not able to explain this with currently understood physics.

Phase transitions often involve a system going out of equilibrium, and we will see how these out-of-equilibrium phenomena could result in gravitational waves. These gravitational waves would then travel unimpeded to our detectors, letting us see back even further in time than the earliest detectable photons – the cosmic microwave background (CMB) – which formed 380 000 years after the Big Bang.

---

\*Durham University, United Kingdom, djuna.lcroon@durham.ac.uk

†Department of Physics and Helsinki Institute of Physics, P.O. Box 64, FI-00014 University of Helsinki, Finland, david.weir@helsinki.fi



Figure 1: Fog and sea ice in the Arctic Ocean. As water vapour – the gaseous phase of water – cools, it condenses to form clouds of liquid water such as the fog seen here. Water, when it cools still further, freezes to form ice. The condensation and freezing of water are two everyday examples of first order phase transitions.

Collider experiments at the LHC, and other experimental particle physics projects are looking to probe the properties of the Higgs boson – as well as trying to discover as-yet unseen new particles or phenomena. These might be hitherto unseen extensions of the Standard Model of particle physics. They could also comprise the sought-after dark matter.

Piecing together a theory from what experimental particle physicists observe might tell us what sort of phase transitions to expect early in the universe’s history. Conversely, detecting gravitational waves from early universe phase transitions would inform where and how to look for new particle physics. And both might shed some light on important open questions such as the origins of dark matter, or the matter-antimatter asymmetry in the universe. It is this *complementarity* between different areas of research that we want to highlight in the current work.<sup>1</sup>

In this section we begin by reviewing the history of the universe in broad terms, and the events which could have led to production of gravitational waves. In Section 2 we will go into more detail of the theory of early universe phase transitions, and the reasons they could have taken place. In Section 3 we review what gravitational waves are, and how they can be produced by phase transitions in the early universe. This is followed by Section 4, in which we discuss ways in which the physics of the early universe can be probed – principally through gravitational waves, but also colliders like the LHC. We conclude and give an outlook in Section 5.

## 1.1 Early universe physics - a brief history of what we know

Let us first start by reviewing what we already know about the history of the universe, aided by Fig. 2.

Our cosmic journey starts with *inflation*, a period of exponential expansion of space when the universe was between  $10^{-36}$  –  $10^{-32}$  seconds old (for an introductory review, see [7]). Inflation was originally proposed in Ref. [8] to solve some of the problems with the Big Bang model,<sup>2</sup> but also explains the origin of structure in the universe: quantum fluctuations, enhanced by inflation, can form the seeds of galaxies.

Inflation ends with a somewhat short period called *reheating* in which the universe fills up with thermal

---

<sup>1</sup>See Ref. [6] for a discussion of other ways in which electroweak-scale physics can have an impact on the universe’s evolution.

<sup>2</sup>Namely the observation of very similar temperatures across causally disconnected regions of the sky (the horizon problem), the extreme flatness of the metric of space-time (the flatness problem) and the non-observation of magnetic monopoles and other relics [9].

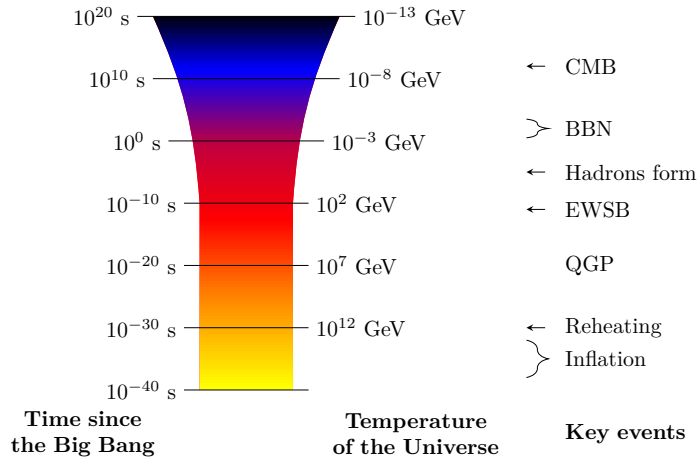


Figure 2: Chronology of the very early universe. The key events discussed in Section 1.1 are shown, along a logarithmic timeline. The relationship between time and temperature shown here assumes that the energy density of radiation dominates the universe’s expansion, and that there are no additional degrees of freedom beyond those known about in the Standard Model of particle physics. Various events in the history of the universe could have produced gravitational waves, see Table 1.

decay products of the *inflaton*, a particle which is thought to be responsible for driving the period of inflation. After reheating, the universe contains a hot primordial soup of mostly quarks and gluons, called the quark-gluon plasma. This lasts until the temperature of the universe cools beyond the QCD-scale (marked “Hadrons form” in Fig. 2), and quarks combine into *hadrons*: protons and neutrons (mostly). Through a currently undetermined process, there are more hadrons than anti-hadrons, such that they do not annihilate immediately. This is the big matter-antimatter asymmetry mystery mentioned above.

You will note another scale on Fig. 2, above the QCD scale, with the acronym EWSB. That stands for *Electroweak Symmetry Breaking* (an introduction can be found in Ref. [10]), and corresponds to the scale at which the Higgs particle gave mass to the particles of the SM. This mass mechanism is a good example of a process which can give rise to a phase transition. We will study it in detail in Section 2.4.1.

During the era of *Big Bang Nucleosynthesis* (BBN) the light elements are produced from the protons and the neutrons (for an introduction, see Ref. [11]). The plasma is still ionised at this time, however. Besides hydrogen and helium, it contains small amounts of deuterium, helium-3, helium-4, and lithium-7 as well. The primordial abundances of these elements can be measured today, and are used to test theories of the early universe.

After BBN, the primordial soup contains ionised nuclei, electrons, and photons, until it further cools down. In the era of *recombination* it becomes energetically favoured for the electrons to bind to the nuclei to form stable atoms. As a result, the photons are more free to travel without continuously bumping into electrons: the universe becomes transparent. These newly released photons are still observable today: they form the CMB, our earliest direct probe of the universe to date

## 1.2 Primordial particle physics

As can be seen in Fig. 2, the early universe was very hot. At these temperatures, it contains a plasma of gamma rays (very energetic photons), and other particles with a temperature dependent composition. To study this plasma in detail, we first need to consider how particles behave at high temperatures. The high temperature implies that the gamma rays zooming around in the plasma can spontaneously create combinations of particles and antiparticles with a combined rest energy smaller than its energy. Conversely, when a particle crosses paths with its antiparticle, they can annihilate back into a photon. If these processes

Event	Time/s	Temp/GeV	$g_*$	Frequency/Hz
QCD phase transition	$10^{-3}$	0.1	$\sim 10$	$10^{-8}$
EW phase transition	$10^{-11}$	100	$\sim 100$	$10^{-5}$
?	$10^{-25}$	$10^9$	$\gtrsim 100$	100
End of inflation	$\gtrsim 10^{-36}$	$\lesssim 10^{16}$	$\gtrsim 100$	$\gtrsim 10^8$

Table 1: Relationship between the temperature of the early universe, the approximate number of relativistic degrees of freedom  $g_*$  (see Ref. [13]) at the time gravitational waves were being produced, and the typical frequency of gravitational waves produced (assuming they are produced on cosmological scales), after Refs. [14, 15]. The final column can be found by substituting the quantities into Eq. (38) with  $B \sim 0.1$ .

occur at the same rate, the particle species is in thermal equilibrium with the early universe plasma. As the temperature drops, the average plasma energy may fall below the rest mass of a particle and its antiparticle. When that happens, it will no longer be possible to create the pair. We say that the particles decouple from the plasma.

The dropping temperature also affects how particles interact with other particles, how they propagate (i.e. what their effective mass is), and sometimes even how particles are defined. The change in behaviour of particles and interactions as the temperature changes is very important to study the physics of the early universe. We know that some important things must have happened when the universe was cooling down. Besides the processes we can confidently mark on our cosmic timeline, some currently unknown events must have occurred, answering open questions in particle physics. A good example is the unknown process producing the abundance of protons over anti-protons, which survived until today (the proton is stable<sup>3</sup>): the matter-antimatter asymmetry. Moreover, we know that some time in the first second, *dark matter* must have originated: it may have been in thermal equilibrium and then decoupled, or it may have formed in another way. As it has eluded many dedicated experiments today, its behaviour in the early universe may hold the key to its nature.

These two big theoretical questions – the origins of the matter-antimatter asymmetry, and the nature of dark matter – motivate particle physicists and cosmologists to study the early universe, theoretically as well as experimentally. In the next few subsections we will explore the ways in which we may gather information.

### 1.3 Experimental information from the early universe

Experimentally, we have a few different ways of learning about the early universe. The temperature fluctuations in the photons of the CMB are the best explored probe of observational information. It has taught us, for example, how much dark matter there is compared to luminous matter; how many light (relativistic) degrees of freedom there were in the early universe, and it helps us understand the cosmic expansion history.

The CMB comprises the earliest photons we can detect, resulting from the moment that the universe turned from opaque to transparent (to photons).<sup>4</sup> Before this time, the photons were in thermal equilibrium with the rest of the primordial soup. In thermal equilibrium, temperature fluctuations get washed out, and therefore the CMB can be seen as a snapshot of the universe at the time when photons decoupled from the primordial plasma, 380 000 years after the Big Bang.

Nevertheless, in contrast to photons, gravitational waves were never in thermal equilibrium with the rest of the plasma. Therefore, after a gravitational wave is produced, it travels through space more or less unimpeded. Therefore a stochastic gravitational wave background (SGWB) could contain direct information from much earlier times than the CMB does. In this way, particle physics and cosmology are directly connected to searches for gravitational wave backgrounds.

If there were strong enough sources of gravitational waves in the early universe, they could therefore be our earliest – and highest-energy – probes of fundamental physics (see Table 1). Now, what types of events

<sup>3</sup>This has been experimentally confirmed to very high accuracy in the SM, see the baryon properties tables in Ref. [12].

<sup>4</sup>The corresponding distance is called the surface of last scattering.

could source gravitational radiation, and why do we expect them to have happened? There are types of candidate scenarios, which have a few things in common: inhomogeneity, and the release of a lot of energy in a non-spherically symmetric way (we will come back to this in Section 3). Here, we will focus on first-order phase transitions.

A phase transition is an event in which certain properties of a thermodynamic system change. An example from particle physics is the Higgs mechanism, in which the particles of the Standard Model (except the photon and the gluons) obtained a mass, when our universe was about  $10^{-11}$  seconds old. Phase transitions can be classified by their *order*: we are interested in first order phase transitions, in which there is a departure from thermal equilibrium and latent heat is released.

As you can imagine, there are many candidate theories in which the properties of particles imply a phase transition happened in the early Universe. Such theories are often related to fundamental open questions in particle physics. For example, the question why there is more matter than antimatter in our universe can only be answered by an early universe event which includes a departure from equilibrium. Another open question relates to the elusive substance we call dark matter: gravitational waves may be one of the only ways to shed light on it. We will discuss both of these examples (and a few others) in Section 2.4.

In the rest of this paper we will explain the thermodynamics of a cosmic phase transition, and give examples of classes of models in which such events occur. After a short primer on gravitational waves, we will explain how they are generated in a phase transition. We will finish with a survey of detection strategies, and an outlook to the next generation of experiments.

## 2 Cosmic phase transitions

### 2.1 Spontaneous symmetry breaking

Particle physics studies the most basic building blocks of nature. A great triumph of the last century was the discovery that the fundamental particles we know about, and how they interact with each other, can be organised in a simple set of rules. The success of these rules has been demonstrated by their prediction of new fundamental particles, which were indeed subsequently found.

The organising principles of particle physics are more commonly referred to as symmetries. That is because of the mathematical definition of a symmetry: a feature that remains conserved or unchanged under a transformation. For example, if your face happened to be perfectly left-right symmetric, the transformation of flipping your face through the vertical axis in the middle would result in exactly the same face. An example from particle physics is the conservation of electromagnetic charge, with the corresponding electromagnetic symmetry. Conserved quantities also come with a force, such as the repulsive force between two like (electromagnetic) charges.

In some cases, the symmetries of particle physics depend on the energy scale. As the universe cools, a high-energy symmetry may not be present in the low-energy physics. Typically, the symmetry is technically still present in the theory, but the vacuum state does not reflect it: we say the symmetry is spontaneously broken. The spontaneous breaking of symmetries is intimately related to first order phase transitions, so we will take a moment to review this.

As an example of a theory that features spontaneous symmetry breaking, we can take the Abelian Higgs model in scalar electrodynamics.<sup>5</sup> The potential energy of the Abelian Higgs particle is described by,

$$V(\Phi) = -m^2\Phi^\dagger\Phi + \lambda(\Phi^\dagger\Phi)^2 \quad (1)$$

where  $\Phi$  is complex,  $\Phi = |\Phi|e^{i\alpha}$  (here  $\alpha$  is a real parameter). Clearly,  $V(\Phi)$  is invariant under shifts in  $\alpha$ :

$$V(|\Phi|e^{i\alpha}) = V(|\Phi|e^{i(\alpha+\delta\alpha)}). \quad (2)$$

---

<sup>5</sup>In this model, a phase transition can result in the formation of topological defects known as cosmic strings (see e.g. [16]), but that is not the focus of the current work.

You may also have noticed that the lowest value of  $V(\Phi)$  (the vacuum) is not reached at  $|\Phi| = 0$ , but rather at  $|\Phi| = v \equiv m/\sqrt{2\lambda}$ , as also demonstrated in Fig. 3 (left). From that figure you can also tell that the potential has rotational symmetry about the origin (mathematically, this is called U(1) symmetry), but not about a vacuum state: the symmetry is spontaneously broken.<sup>6</sup>

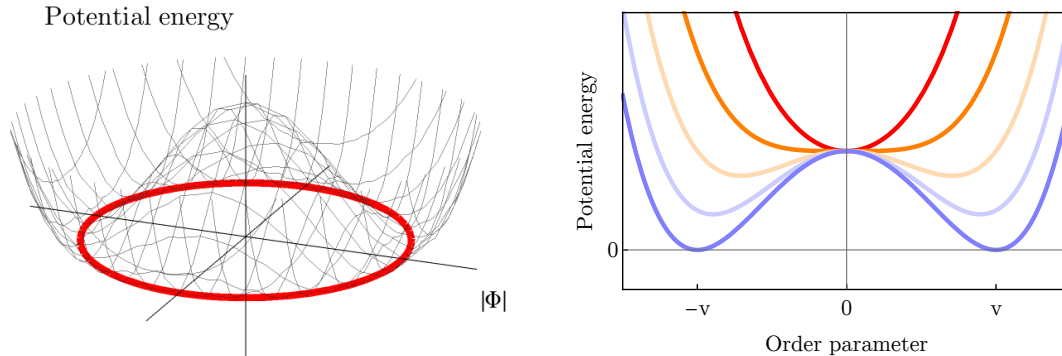


Figure 3: Symmetry breaking potential of the Abelian Higgs model, resembling the underside of a wine bottle. *Left:* Though the potential is symmetric, the vacuum (indicated in red) is not at  $|\Phi| = 0$ , indicating spontaneous symmetry breaking has taken place. *Right:* Cross section of the potential at various temperatures: at high temperature (red line), the lowest energy state is symmetric about the zero axis. At low temperature (blue lines) the lowest energy states are not symmetric, even though the potential energy curve is.

Things get more interesting when we embed our Abelian Higgs field in a plasma of particles, and we heat that plasma up to temperature  $T$ . Typically, the finite temperature implies that the Higgs particles get ‘kicks’ from other (Higgs) particles, which affect the potential energy in a way that at high temperatures, to first order can be approximated as an effective mass,

$$V(\Phi, T) = (-m^2 + T^2)\Phi^\dagger\Phi + \lambda(\Phi^\dagger\Phi)^2. \quad (3)$$

An illustration is given in the right panel of Fig. 3 (for ease of viewing, we show a slice in the 2d plane at, say,  $\alpha = 0$ ). From (3) we find that if  $T^2 \geq m^2$ , the vacuum state of the theory is indeed at  $|\Phi| = 0$ .

Now, the picture is starting to emerge. In the hot, early universe plasma, the temperature corrections to the potential energy of a field like the Abelian Higgs imply that the potential has a vacuum that respects the symmetry. But as the temperature falls below the other parameters of the potential (in this case  $m$ ), the vacuum shifts. This change in vacuum state is what we call a phase transition. The Higgs vacuum value is here an order parameter: it tracks if the phase transition has happened.

## 2.2 First order phase transitions

In the example above, the finite temperature behaviour is clear: for  $T^2 \geq m^2$  the vacuum is at  $|\Phi| = 0$ , for smaller temperatures, it gradually shifts away (try it!). We call such a continuous shift in vacuum state a second order phase transition. Second order phase transitions are relatively common in theories of particle physics, but also relatively uninteresting: as we will see below, to leave an imprint a sudden release of energy is needed.

Such a sudden release of energy is a feature of a first order phase transition. In the language of the shifting vacuum expectation value  $|\Phi|$ , it implies a discontinuity. Consider for example the alternative potential energy of  $\Phi$  at high temperatures,

$$V(|\Phi|, T) = (-m^2 + T^2)|\Phi|^2 - T|\Phi|^3 + \lambda|\Phi|^4, \quad (4)$$

<sup>6</sup>You can show this mathematically using the Abelian Higgs potential, by writing  $\Phi = v + \delta\Phi$ .

a simplified example which captures the essential behaviour of some theories we will describe in the next section. At very high temperatures, the vacuum state of this potential is at  $\phi = 0$ . But for intermediate temperatures, specifically for  $m < T < 2m\sqrt{\lambda}/\sqrt{4\lambda - 1}$  the lowest energy state is away from  $\phi = 0$ , and separated from it by a barrier. This situation is illustrated in Fig. 4.

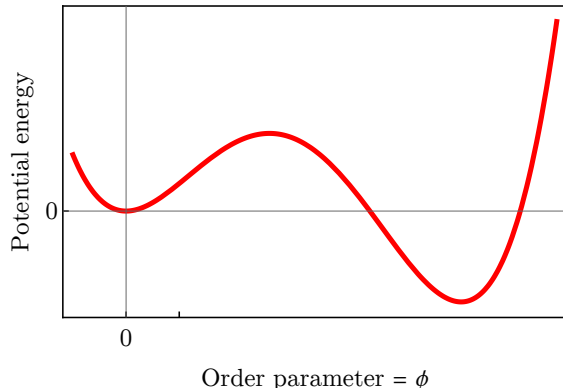


Figure 4: Form of the potential (4) at an intermediate temperature  $m < T < 2m\sqrt{\lambda}/\sqrt{4\lambda - 1}$ .

It is clear that in this type of scenario, the evolution from the symmetric to the broken vacuum is not smooth. If it happens at all, it proceeds via the quantum process of tunnelling through the barrier, or through a thermal fluctuation over the barrier. In the next subsection we will outline the formalism that captures both of these processes.

### 2.3 Bubble nucleation

To describe the phase transition, we first need to calculate the probability for tunnelling through the potential barrier. In one-dimensional, non-relativistic quantum mechanics, such a tunnelling probability can be found using the semi-classical WKB approximation, which gives

$$\frac{d^2\psi}{dx^2} - 2m(V(x) - E)\psi = 0, \quad (5)$$

where  $E$  is the energy of the state and  $V(x)$  is the potential energy as a function of position  $x$  (here, as in the rest of the article, we have set  $\hbar = 1$ ). For constant potential, this is solved by  $\psi \propto \exp(-ikx)$  where  $k = \sqrt{2m(E - V)}$ , i.e. a plane wave, for varying potential this can be generalised to  $\psi \propto \exp(-i \int k(x) dx)$  with  $k(x) = \sqrt{2m(E - V(x))}$ . If  $\psi$  has smaller energy than the potential between points  $x_1$  and  $x_2$ , it is exponentially decreasing, with associated tunnelling rate

$$\Gamma_{\text{WKB}} \propto e^{-\int_{x_0}^{x_1} \sqrt{2m(V(x) - E)} dx}. \quad (6)$$

It turns out that we can use something analogous in quantum field theory, the extension of quantum mechanics to relativistic systems: a method called the bounce method [17, 18]. Indeed, we can go to Euclidean space, where the theory is described by the action

$$S_E = \int d^d x_E [(\partial_{x_E} \phi)^2 + V(\phi, T)] \quad (7)$$

in which the subscript  $E$  denotes Euclidean and the integral is over Euclidean space. The dimension of this integral is  $d = 4$  for quantum tunnelling (a phase transition happening at zero temperature) and  $d = 3$  for a thermal phase transition – in equilibrium thermal field theory in Euclidean space, the time dimension is compact and inversely proportional to the temperature, effectively reducing the dimensionality of problem. As usual, the equations of motion are derived from extremising this action. Because solutions that extremise

the energy are expected to be spherically symmetric, the only relevant coordinate is the radial one:  $r = \sqrt{x_E^2 + y_E^2 + z_E^2}$ . We may therefore simplify our equations of motion to become,<sup>7</sup>

$$\frac{d^2\phi}{dr^2} + \frac{d-1}{r} \frac{d\phi}{dr} = \frac{dV(\phi, T)}{d\phi} \quad (8)$$

with boundary conditions,

$$\begin{aligned} \phi(r \rightarrow \infty) &= 0, \\ \left. \frac{d\phi}{dr} \right|_{r=0} &= 0. \end{aligned} \quad (9)$$

ensuring finite energy at the origin and vanishing  $\phi$  at infinity.

To find the false vacuum decay rate, the solution to (8) with (9) can be substituted back into the Euclidean action. The decay rate per unit volume will be depend on this result,<sup>8</sup>

$$\Gamma = A(T)e^{-S_E T^{4-d}} \quad (10)$$

where dimensional analysis can be used to show  $A(T) \sim T^4$  and  $S_E$  is the Euclidean action (7) evaluated on the solution to Eqs. (8) and (9). For thermal fluctuations, although the solution will itself depend on temperature, it is generally the case that the nucleation rate increases exponentially as the temperature decreases, because the ratio  $S_E/T$  decreases with temperature.

## 2.4 Models with first order phase transitions

### 2.4.1 The Electroweak Phase Transition

In the last section, we discussed how phase transitions are often related to the spontaneous breaking of symmetries. In the Standard Model of particle physics, one such spontaneous breaking occurred in the early universe. In this phase transition, the order parameter was the Higgs boson, and the process is responsible for giving mass to all particles that couple to the Higgs, including itself. It is easy to see how that works, imagine for example the Higgs boson  $\phi$  coupling to two fermionic particles (for example quarks, or electrons)  $\psi$ :

$$\mathcal{L} \supset -y\phi\bar{\psi}\psi \quad (11)$$

here  $y$  is a constant and  $\mathcal{L} \supset$  implies that this interaction is part of the Lagrangian of the theory.<sup>9</sup> Now imagine that the Higgs field changes vacuum state, from  $\phi = 0$  to another value  $\phi = v$ . Then, we may expand  $\phi = v + \delta\phi$  (where  $\delta\phi$  is a fluctuation around the vacuum),

$$\mathcal{L} \supset -(yv\bar{\psi}\psi + y\delta\phi\bar{\psi}\psi) \quad (12)$$

The first term on the right hand has two fermions and a constant ( $yv$ ), and it defines the newly acquired mass of the fermion. The second term is again an interaction between  $\psi$  and the dynamical field  $\delta\phi$ .

Now that we have established that a phase transition was responsible for the mass mechanism in the Standard Model, you may wonder what its order was. It is possible to calculate how the theory changes with temperature, like we demonstrated in Fig. 3. This will depend on all the particles of the Standard Model that interact with the Higgs. It so happens that with just the properties of the detected particles of the Standard Model, the phase transition is not first order: while there is an effective  $\phi^3$  interaction at finite temperatures as in (4), it comes with a small coefficient, such that the barrier is not large enough to separate the vacua at finite temperature (try putting in a small coefficient to see that that is the case!). But the order

<sup>7</sup>You are encouraged to derive these from the action (7) using the Euler-Lagrange formalism.

<sup>8</sup>For further reading on the decay rate, see [19–21].

<sup>9</sup>The bar implies a Dirac conjugate transpose,  $\bar{\psi} \equiv \psi^\dagger \gamma^0$  where  $\gamma^0$  is a Dirac matrix, but that is not important for the present discussion.



of the phase transition could change if new, currently undiscovered particles lurk around the corner. This is because interactions with new particles may imply effective additional terms in the Higgs potential, such as for example

$$\mathcal{L} \supset -\frac{1}{\Lambda^2} \phi^6 \tag{13}$$

where  $\Lambda$  has dimensions of energy, such that the Lagrangian density still has dimensions of energy to the fourth power. With this extra effective term, a double well potential may be realised even without a temperature-dependent interaction.

At this point you may object that if the existence of a gravitational wave spectrum from the phase transition relies on the hypothesis of new particles, it seems somewhat improbable. But there is a very good reason why cosmologists think there was a first order phase transition in the early universe, because it may help explain why there is more matter than antimatter in the universe, as we briefly alluded to in Sections 1.2 and 1.3. Any theory that proposes an explanation of the matter-antimatter asymmetry must have certain features, first formulated by Andrei Sakharov in 1967. Importantly, one of those conditions identifies the need for out of (thermal) equilibrium dynamics. To see that that is necessary, imagine a process that is responsible for biasing matter over antimatter - in thermal equilibrium, this process could happen in both directions and therefore erase the asymmetry. First order phase transitions are good examples of reactions out-of-thermal-equilibrium, and the Higgs mechanism constitutes one of the phase transitions we are sure did occur in the early Universe. Besides, the Higgs interacts with the other particles of the Standard Model in such a way as to make the creation of the matter asymmetry possible in many different models of the phase transition. Theories of this kind are called Electroweak Baryogenesis; electroweak after the symmetry broken by the Higgs, and baryogenesis after the genesis of baryons (matter).<sup>10</sup>

### 2.4.2 Hidden sectors

In the last subsection, we talked about a phase transition that must have happened in the early universe involving the particles we have discovered to exist today, belonging to the Standard Model of particle physics. However, answering the big open questions that still exist typically requires the existence of additional particles, or interacting *sectors* of additional particles, which are sometimes referred to as *hidden* or *dark* sectors. They are given those names because their interaction with the SM particles (including with photons) cannot be very strong, or we would have discovered them by now. However, we do know that a hidden sector which explains the existence of dark matter must interact gravitationally. Therein lies the interest in gravitational wave studies: it may be one of very few windows onto the nature of dark matter.

As we explained in the previous subsection, a phase transition involving the SM Higgs boson explains the generation of mass in the early universe. This phase transition may have been first order due to the presence of new particles. A hidden sector has to be massive, too, to interact with gravity and explain dark matter. So it is also possible that a corresponding dark Higgs-like mechanism gave rise to a first order phase transition. A Higgs-like mechanism in the dark sector is different from the SM Higgs mechanism described in the previous subsection, because we know quite a lot about the latter: we know the Higgs mass (at zero temperature), and we know the value of its vacuum expectation value (again, at zero temperature). We also know how the Higgs couples to the other particles of the SM. All these pieces of information mean that the phase transition is quite constrained: we know it must have happened at a temperature of about 100 GeV, for example, implying a GW spectrum peaking at roughly  $10^{-5}$  Hz. We have also learned some things about what additional particles could *not* exist (through studies at the Large Hadron Collider, for example), which tells us some more. None of this is true for a potential phase transition in a hidden sector. In fact, proposed dark matter particles exist for a vast range of masses: from  $10^{-22}$  eV to macroscopic objects of the mass of the sun,  $10^{66}$  eV. There could be one such type of particle, or many, and they could be interacting, or not.

It may seem that with all these open questions about hidden sectors, we do not know what we are looking for. However, as we will see in the next section, gravitational waves from phase transitions follow a very distinctive spectrum, independent on the microphysics that gave rise to the transition. This insight makes it

---

<sup>10</sup>If you are interested in reading further on this topic, we recommend [22].

possible to study what can be learned about hidden sectors from such transitions, which is an ongoing effort by the scientific community.

### 2.4.3 Confinement

The third type of early universe phase transition we will consider is a bit different: instead of a field like the Higgs boson obtaining a vacuum expectation value, it occurs when particles *confine*. You may have wondered what keeps the quarks bound together inside a proton or neutron (the collection of such things is called a hadron), and you may have heard that a strong nuclear force is exerted between them, which increases with the distance between the quarks. This strong force ensures that the quarks are confined inside hadrons, inside of which they are free to move around: this is called asymptotic freedom.

But what does a force which increases with distance mean in the context of the early universe? Well, in quantum field theory, short distances correspond to higher energy. So in the very early universe, temperatures were reached which implied that the quarks roamed around freely, in the quark gluon plasma. As the universe cooled, the quarks started to become bound up into the hadrons, a process we call the QCD phase transition (we mentioned it in Table 1). It is pretty difficult to work out what the order of that transition was, but it will probably depend on the number of free quarks there were in the plasma:  $N_f$ . For the SM,  $N_f = 3$ : three of the six quarks (the top, the bottom, and the charm quark) are so heavy that they would have decoupled before the phase transition.<sup>11</sup> The scientific consensus at this time, based on detailed lattice simulations, is that for the SM, the QCD phase transition is not first order, but if for any reason there are more light quarks in the plasma at the time of transition, that conclusion could potentially be reversed. The same holds for a dark sector with a similar confining mechanism as in QCD. So, as in the two subsections above, a first order phase transition in the early universe is an indication that we are onto new particle physics, beyond the standard model.

## 3 Gravitational Waves

### 3.1 Ripples in spacetime

Gravitational waves are solutions to a wave equation, where the source term is given by the *energy-momentum tensor* of the GW-source.<sup>12</sup> The *metric tensor*  $g_{\mu\nu}$  is the key object of study in the theory of general relativity. We can expand about some background spacetime, which we take to be flat, Minkowski spacetime with metric  $\eta_{\mu\nu}$  and consider small fluctuations  $h_{\mu\nu}$ :

$$g_{\mu\nu} = \eta_{\mu\nu} + h_{\mu\nu}, \quad |h_{\mu\nu}| \ll 1 \quad (14)$$

Using Einstein's equations of general relativity, we arrive at the wave equation for the so-called *metric perturbations*  $h_{\mu\nu}$ :

$$\square h_{\mu\nu} = -\frac{16\pi G}{c^4} T_{\mu\nu}^{\text{TT}}, \quad (15)$$

where the  $\square$  operator is the d'Alembertian:  $\square = \partial_\mu \partial^\mu$  and where the Greek indices run over space-time dimensions:  $\mu, \nu = 0, 1, 2, 3$ . This is a second-order differential (wave) equation, with a source:  $T_{\mu\nu}$ , the *energy momentum tensor*. We will not show its derivation here, but it follows directly from Einstein's field equations for general relativity.

The superscript TT denotes that we have to take the transverse-traceless part of the energy-momentum tensor. In other words, only perturbations that are transverse to the propagation direction and traceless in terms of the tensor indices  $\mu$  and  $\nu$  source physical gravitational waves. If we consider  $h_{\mu\nu}$  to be a

<sup>11</sup>For one (the strange quark) it is borderline, so sometimes it is written  $N_f = 2 + 1$ .

<sup>12</sup>See e.g. Refs. [23, 24] for more detailed introductions to this equation and the solutions discussed in this section. If you are not familiar with index notation of linear algebra, we recommend you to review it before reading the next sections.

monochromatic travelling wave in the  $x$ -direction, it will take the form

$$h_{\mu\nu} = \left[ h_+ \begin{pmatrix} 0 & 0 & 0 & 0 \\ 0 & 0 & 0 & 0 \\ 0 & 0 & 1 & 0 \\ 0 & 0 & 0 & -1 \end{pmatrix} + h_\times \begin{pmatrix} 0 & 0 & 0 & 0 \\ 0 & 0 & 0 & 0 \\ 0 & 0 & 0 & 1 \\ 0 & 0 & 1 & 0 \end{pmatrix} \right] e^{ikx}. \quad (16)$$

which is only nonzero in the  $y$ - and  $z$ -directions (transverse) and, as a matrix, has zero trace. The  $h_+$  and  $h_\times$  are the two polarisation components. In practice, gravitational waves from both astrophysical sources and the cosmological background are superpositions of polarisations, frequencies, amplitudes and directions of propagation – just as is the case for electromagnetic radiation from astrophysical and cosmological sources.

This linear wave equation can be solved by a retarded Green's function, which you will have come across in electrodynamics. The solution will only feature spatial dimensions, as the temporal contribution can be related to it using energy-momentum conservation. It is in general not very insightful - but in many cases, we can study its behaviour by taking a limit. In particular, if the distance  $r$  to the source is large and the motion inside the source is non-relativistic (moving at a speed much less than the speed of light,  $v \ll c$ ), an expansion in spherical harmonics becomes possible. The first term in this expansion is the quadrupole, given by

$$h_{ab}^{[\text{quad}]} = \frac{2G}{r} \ddot{Q}_{ab} \quad \text{where} \quad Q_{ab} = \int d^3x \rho(t, \mathbf{x}) \left( x_a x_b - \frac{1}{3} r^2 \delta_{ab} \right) \quad (17)$$

which, as we anticipated, depends only on spatial dimensions:  $a, b = 1, 2, 3$ .  $Q_{ab}$  is the *quadrupole moment* of the source (the dots denote time derivatives), and  $\rho(t, \mathbf{x})$  is a time-varying mass density distribution.

Let's pause for a moment to consider this result: gravitational waves are generated by time-varying sources with a nonzero quadrupole moment. This is different from electromagnetism, in which you have dipole radiation as well. An intuitive way to see the difference is this: in electromagnetism, you have both positive and negative charges. The dipole moment arises from these two different charges. On the other hand, the quadrupole moment arises from the arrangement of sources, and does not depend directly on the sign of the charges. Because mass is the charge of the gravitational force, and mass is positive definite, there is quadrupole radiation while dipole radiation is absent.

The quadrupole moment describes a specific change in how the masses are distributed around their (mutual) centre of mass.<sup>13</sup> In practise, this means:

- Spherically symmetric systems do not generate gravitational waves;
- Static or uniformly moving systems do not generate gravitational waves.

### 3.2 Stochastic gravitational wave backgrounds

The above discussion relates to compact sources, such as what has been detected by LIGO and Virgo to date – and even then, it is just the leading order contribution. For our purposes, however, we wish to think about gravitational waves produced in the very early universe. These gravitational waves are not, in general, produced by isolated compact objects. They would be produced by events happening throughout the universe at around the same time. The assumptions that go into the quadrupole formula do not hold in this context,<sup>14</sup> and we have to consider the full equation (15)

Instead of thinking about the strain  $h$  from a single source as we did in the previous section, here the source term  $T_{\mu\nu}$  comes from non-equilibrium events happening at random anywhere within the Hubble radius (roughly speaking, the observable universe). These will then generate a stochastic time- and space-varying ensemble of metric perturbations  $h_{ij}$ . Therefore it is more helpful to think about the *energy density* of the

<sup>13</sup>The monopole and the dipole describe the total amount of mass, and the distribution of mass away from some centre in some direction. If the centre of mass is picked as the centre, the dipole is zero.

<sup>14</sup>Although influential early works like Ref. [25] did apply the quadrupole approximation to colliding pairs of bubbles.

gravitational waves  $\rho_{\text{gw}}$  for a given process than the strain. Just like propagating electromagnetic waves have energy given by the sum of the squares of the electric and magnetic fields, the energy in gravitational waves  $\rho_{\text{gw}}$  is given by the square of the time derivative of the metric perturbations,

$$\rho_{\text{gw}} = \frac{1}{32\pi G} \left\langle \dot{h}_{ij}(\mathbf{x}, t) \dot{h}_{ij}(\mathbf{x}, t) \right\rangle. \quad (18)$$

Here the angle brackets denote that this is an average over some spatial volume (which must be much larger than the typical wavelength of the gravitational waves for the energy to be well defined [26, 27]). We can normalise  $\rho_{\text{gw}}$  to the critical energy density

$$\rho_c = \frac{3H^2}{8\pi G} \quad (19)$$

in the universe at the time to get  $\Omega_{\text{gw}}$ , a cosmological density parameter analogous to for example  $\Omega_{\text{rad}}$  for radiation.

What is often known to cosmologists as the gravitational wave power spectrum is the quantity  $\frac{d\Omega_{\text{gw}}(f)}{d \log f}$  (sometimes shortened to  $\Omega_{\text{gw}}(f)$ ) – the scaled energy density of the universe in gravitational waves per logarithmic frequency interval,

$$\frac{d\Omega_{\text{gw}}(f)}{d \log f} = \frac{1}{\rho_c} \frac{d\rho_{\text{gw}}(f)}{d \log f}, \quad (20)$$

where  $\frac{d\rho_{\text{gw}}(f)}{d \log f}$  is defined through

$$\rho_{\text{gw}} = \int_0^\infty \frac{df}{f} \frac{d\rho_{\text{gw}}(f)}{d \log f}. \quad (21)$$

Note that these formulae relate to the time at which the gravitational waves were produced, or shortly afterwards. They must be cosmologically redshifted to today if we are to make predictions about what might be observed by gravitational wave detectors.

In the next section we will investigate some general rules for what form  $\frac{d\Omega_{\text{gw}}(f)}{d \log f}$  can take, and how the frequency and amplitude get redshifted to today.

### 3.3 General principles for gravitational waves from primordial physics

In order to understand the redshifting to today, we need to understand some cosmology. A universe which is homogeneous and isotropic (but not necessarily static) is described by the Friedman-Lemaître-Robertson-Walker metric, a solution to the Einstein field equations. The dynamics of a cosmological fluid of energy density  $\rho$  and pressure  $p$  are described by the Friedman equations:

$$\frac{\dot{a}^2 + kc^2}{a^2} = \frac{8\pi G\rho + \Lambda c^2}{3}, \quad (22)$$

$$\frac{\ddot{a}}{a} = -\frac{4\pi G}{3} \left( \rho + \frac{3p}{c^2} \right) + \frac{\Lambda c^2}{3}. \quad (23)$$

These equations describe the evolution of  $a$ , the scale factor of the universe, as a function of the energy density, pressure, curvature  $k$  and the cosmological constant  $\Lambda$ . The combination  $\dot{a}/a \equiv H$  is also called the Hubble factor or Hubble rate. Unless  $\Lambda$  or  $k$  dominate, the Friedman equations are solved by  $a \propto t^{\frac{2}{3(1+w)}}$ , where  $w = p/\rho c^2$  is the equation of state parameter of the dominant fluid (we will assume a flat universe without a cosmological constant, meaning that  $\Lambda = k = 0$  in what follows). In the early universe, the most important cosmological fluid was relativistic and behaved like radiation, which yields  $w = 1/3$  (known as the era of *radiation domination*). So as time progressed, the universe expanded.

The expansion of the universe has implications for the particles in our plasma, in particular for radiation. We are interested in gravitational waves produced in the early universe. Produced at a frequency  $f_*$ , they get redshifted on their way to us by the ratio of scale factors then (time  $t_*$ ),  $a(t_*)$ , and now (time  $t_0$ ),  $a(t_0)$ , giving [14, 15, 28]

$$f_0 = \frac{a(t_*)}{a(t_0)} f_*. \quad (24)$$

We can express this relation in terms of temperature (then  $T_*$ , now  $T_0$ ) by assuming entropy,  $s$ , is conserved as the universe expands:

$$s(t)a(t)^3 = \text{constant}. \quad (25)$$

The first law of thermodynamics lets us relate entropy density to energy density, pressure and temperature,

$$s = \frac{\rho + p}{T}, \quad (26)$$

noting that  $p = \rho/3$  for a relativistic fluid. Then,  $\rho$  (and  $p$ ) can be calculated for each hot, ultrarelativistic fermion and boson degree of freedom in the early universe plasma from the Fermi-Dirac and Bose-Einstein distributions respectively (see e.g. Ref. [29]), with energy densities per degree of freedom  $g$

$$\frac{\rho_{\text{bosons}}}{g} = \frac{\pi^2}{30} T^4, \quad \frac{\rho_{\text{fermions}}}{g} = \frac{7}{8} \frac{\pi^2}{30} T^4. \quad (27)$$

Defining an effective number of relativistic degrees of freedom  $g_{*,s}(T)$  that accounts for the factor of 7/8 in (27) and the possibility that some species have decoupled and are no longer in thermal equilibrium with the others, using these expressions in (26) yields<sup>15</sup>

$$s = \frac{2\pi^2}{45} g_{*,s}(T) T^3, \quad (28)$$

and hence using (25),

$$\frac{a(t_*)}{a(t_0)} = \left( \frac{s(t_0)}{s(t_*)} \right)^{\frac{1}{3}} = \left( \frac{g_{*,s}(T_0)}{g_{*,s}(T_*)} \right)^{\frac{1}{3}} \frac{T_0}{T_*}. \quad (29)$$

The number of relativistic degrees of freedom has not changed since the CMB formed, so we can set the temperature today  $T_0$  as the CMB temperature today, 2.726 K and the number of effective relativistic degrees of freedom as  $g_{*,s}(T_r) = 3.91$  [13]. We can then express the ratio of scale factors in terms of electronvolts, by first multiplying the temperature by Boltzmann's constant  $k_B$  to get an energy, and then dividing by the elementary charge  $e$ , giving  $T_0 = 234.4 \mu\text{eV}$ . Since we want to express the ratio<sup>16</sup> in Eq. 29 in terms of 100 GeV (the approximate temperature when the electroweak transition happened) and  $g_{*,s} \sim 100$  (the approximate number of effective relativistic degrees of freedom at the same time) we end up with a prefactor

$$\left( \frac{3.91}{100} \right)^{\frac{1}{3}} \times \frac{234.4 \times 10^{-6}}{100 \times 10^9} \approx 8.0 \times 10^{-16} \quad (30)$$

giving the final equation for the redshifted frequency,

$$f_0 \simeq 8.0 \times 10^{-16} \left( \frac{100}{g_{*,s}(T_*)} \right)^{\frac{1}{3}} \left( \frac{100 \text{ GeV}}{T_*} \right) f_*. \quad (31)$$

We can use this formula to work out what frequency gravitational waves produced in the early universe will have been redshifted to today. Let us assume that some large-scale source produces gravitational waves on some scale comparable to the observable universe at the time in question.

Objects at a distance given by the inverse Hubble rate,  $H_*^{-1}$  are receding at the speed of light, so any causal process that produces gravitational waves must have a characteristic wavelength  $\lambda \lesssim H_*^{-1}$ . We can use (22) to work out the Hubble rate. Still assuming radiation domination, and defining another<sup>17</sup> effective number of degrees of freedom  $g_*(T)$ , the energy density of the universe is given by

$$\rho(T) = \frac{\pi^2}{30} g_*(T) T^4, \quad (32)$$

<sup>15</sup>Because the combination  $g_{*,s}(T)T^3$  can be thought of as shorthand for a sum over all spin and helicity states and their respective temperatures,  $g_{*,s}(T)$  is not always an integer—it will contain factors compensating for the different prefactors of fermions and bosons, as well as the possible different temperatures of different particle species. Furthermore, the ‘s’ subscript means it is specific to the entropy measurement (which carries a  $T^3$  factor).

<sup>16</sup>This is purely for convenience; the equation still works for other events in the early universe, too.

<sup>17</sup>This measure  $g_*$  is specific to measurements of energy density, carrying a  $T^4$  factor compared to the  $T^3$  factor of  $g_{*,s}$ .

in line with (27). Remembering that we set  $\Lambda = k = 0$  for a flat universe and substituting this into Eq. (22), we find

$$H_*^2 \equiv \frac{\dot{a}(t_*)^2}{a(t_*)^2} = \frac{8\pi G}{3} \rho_* = \frac{8\pi G}{3} \frac{\pi^2}{30} g_*(T_*) T_*^4. \quad (33)$$

Since we are working in units where  $\hbar = c = 1$  and expressing energies and temperatures in eV, it is perhaps helpful to write

$$H_* = \frac{1}{M_{\text{P}}} \sqrt{\frac{\pi^2}{90}} \sqrt{g_*(T_*)} T_*^2, \quad (34)$$

where the reduced Planck mass  $M_{\text{P}} = \sqrt{\hbar c / 8\pi G} = 2.44 \times 10^{18} \text{ GeV}/c^2$ .

Now we cast  $H_*$  in terms of typical numbers for  $g_*$  and  $T_*$  at the electroweak scale:

$$H_* = \frac{1}{M_{\text{P}}} \sqrt{\frac{\pi^2}{90}} (100)^{\frac{1}{2}} \left( \frac{g_*(T_*)}{100} \right)^{\frac{1}{2}} (100 \text{ GeV})^2 \left( \frac{T_*}{100 \text{ GeV}} \right)^2 \quad (35)$$

$$= 1.90 \times 10^9 \left( \frac{g_*(T_*)}{100} \right)^{\frac{1}{2}} \left( \frac{T_*}{100 \text{ GeV}} \right)^2 \text{ Hz}. \quad (36)$$

To get to the second step, we must return to SI units. One way is to convert all the energies and masses from electronvolts to Joules (remembering to also multiply the Planck mass by  $c^2$ ) and then dividing by the reduced Planck constant  $\hbar$  (with units Js) to get a quantity with the right units, Hz.

Next, suppose we take our wavelength  $\lambda_*$  to be some fraction  $B/H_*$  ( $B < 1$ ). The frequency of gravitational radiation emitted will be

$$f_* = H_*/B. \quad (37)$$

Then, we can get an expression in terms of  $B$  for the frequency today by substituting (36) into (37) to work out the frequency of the gravitational waves at the the time, and then using that in (31) to redshift the resulting frequency to today. This yields

$$f_0 = 2.7 \times 10^{-6} \frac{1}{B} \left( \frac{g_*(T_*)}{100} \right)^{\frac{1}{6}} \left( \frac{T_*}{100 \text{ GeV}} \right) \text{ Hz}. \quad (38)$$

More prosaically, this can also be thought of as ‘redshifting’ the Hubble rate from the time of interest to today. If a process produces gravitational waves on length scales close to the Hubble radius, we can take  $B \sim 0.1$  and obtain the typical gravitational wave frequencies of Table 1. We will return to the way in which the scale  $B$  is set in more detail in the next section.

Now we know the frequency at which the gravitational waves are produced, we want to know what amplitude to expect. Gravitational waves behave like radiation, and so their fraction of the energy in the universe scales just the same,

$$\rho_{gw,0} = \rho_{\text{gw}} \left( \frac{a(t_*)}{a(t_0)} \right)^4. \quad (39)$$

Substituting in Eq. (29) gives

$$\rho_{gw,0} = \rho_{\text{gw}} \left( \frac{g_{*,s}(T_0)}{g_{*,s}(T_*)} \right)^{\frac{4}{3}} \left( \frac{T_0}{T_*} \right)^4 \quad (40)$$

$$= \rho_{\text{gw}} \left( \frac{g_{*,s}(T_0)}{g_{*,s}(T_*)} \right)^{\frac{4}{3}} \frac{\rho_{\text{rad},0} g_*(T_*)}{\rho_{\text{rad}} g_*(T_0)}. \quad (41)$$

The energy density during the era of radiation domination is given by Eq. 32, and we have used that in the final equality. We divide both sides by the present day critical energy density  $\rho_c \equiv 3H_0^2/8\pi G$ , and write things in terms of the density parameters, defined as  $\Omega_{\text{gw}} \equiv \rho_{\text{gw}}/\rho_c$  for gravitational waves, and  $\Omega_{\text{rad}} \equiv \rho_{\text{rad}}/\rho_c$  for radiation.

The critical energy density is proportional to  $H_0^2$ . Therefore we also multiply by the *reduced Hubble constant*  $h$ , defined via the present-day Hubble constant  $H_0 = h \times 100 \text{ km s}^{-1} \text{ Mpc}^{-1}$ , so that our results do not directly depend on measurements of the present-day Hubble rate, and because the quoted results for cosmological parameters  $\Omega_i$  are usually of the form  $h^2 \Omega_i$ . We then obtain

$$h^2 \Omega_{\text{gw},0} = h^2 \Omega_{\text{rad},0} \left( \frac{g_{*,s}(T_0)}{g_{*,s}(T_*)} \right)^{\frac{4}{3}} \frac{g_*(T_*) \rho_{\text{gw}}}{g_*(T_0) \rho_{\text{rad}}}. \quad (42)$$

We know the fraction of the present-day universe's energy which is radiation,<sup>18</sup> namely  $h^2 \Omega_{\text{rad},0} \approx 4.18 \times 10^{-5}$ . Again we need  $g_{*,s}(T_r) = 3.91$ , but also  $g_*(T_r) = 3.36$  (the difference being due to the neutrinos being decoupled) [13].

Let us assume that some fraction  $C \ll 1$  of the universe's energy ends up in gravitational waves, such that  $\rho_{\text{gw}}/\rho_{\text{rad}} \approx C$  (we are still assuming the universe is radiation-dominated, which is why we divide by the radiation energy density). For an extremely strong first order phase transition, we could take say  $C \sim 0.1$  (which would be possible if the source were very long-lasting and very efficient). Many processes, including phase transitions, produce gravitational wave spectra that have a clear peak at some frequency, so let us also consider an idealised power spectrum with all the power concentrated close to one frequency  $f_*$ ,

$$\frac{d\Omega_{\text{gw}}(f)}{d \log f} = \frac{\rho_{\text{gw}}}{\rho_c} S(f, f_*). \quad (43)$$

It turns out that the simplest spectral shape  $S(f, f_*)$  which has a single peak and is consistent with physical requirements is a *broken power law* (a Gaussian would tend to a constant for  $f \ll f_*$ , and a Dirac delta function would offer less physical insight). Furthermore, a broken power law is quite close to what simulations and modelling predict for a first-order phase transition. We take [31]

$$S(f, f_*) = \frac{(f/f_*)^3}{1 + (f/f_*)^4}. \quad (44)$$

As explained in Ref. [31], this ansatz also satisfies important physical arguments. It is causal (it looks like white noise at large wavelengths, i.e. small  $f$ , because it goes as  $f^3$ ) and means that there is finite total energy in gravitational waves, i.e.  $S(f, f_*) \rightarrow 0$  as  $f \rightarrow \infty$ . We have chosen here that  $S(f) \propto f^{-1}$  at large  $f$  but this depends on the details of the system (see Section 3.4).

Then, taking  $g_{*,s}(T_*) \approx g_*(T_*)$  and casting in terms of typical electroweak-scale numbers (so that they are both close to 100), the amplitude of gravitational waves today (when the frequency  $f_*$  has become  $f_0$ ) is approximately

$$h^2 \frac{d\Omega_{\text{GW},0}(f)}{d \log f} \approx 4.18 \times 10^{-5} \times \frac{3.91^{\frac{4}{3}}}{3.36} \times 100^{-\frac{1}{3}} \left( \frac{100}{g_*(T_*)} \right)^{\frac{1}{3}} C S(f, f_0) \quad (45)$$

and with our broken power law spectral shape for  $S(f, f_0)$  and  $C \sim 0.1$ ,

$$h^2 \frac{d\Omega_{\text{GW},0}^{\text{ideal}}(f)}{d \log f} \approx 1.65 \times 10^{-6} \left( \frac{100}{g_*(T_*)} \right)^{\frac{1}{3}} \frac{(f/f_0)^3}{1 + (f/f_0)^4}. \quad (46)$$

We can use this last equation and the values in Table 1 to plot generic highest-possible amplitudes for primordial stochastic backgrounds at different energy scales (Figure 5). Note how the peak amplitude of the redshifted present-day power spectrum is only weakly dependent on the time in the history of the universe at which the transition took place, *assuming* a given fraction of the universe's energy participates in the transition.

We will see in Section 4 that the detectability of a signal depends on the signal-to-noise ratio (SNR), not the raw amplitude, which in turn depends on the details of how the signal is being observed. This is because

<sup>18</sup>The cosmic microwave background is very nearly a blackbody, so the energy density parameter for photons  $h^2 \Omega_\gamma$  can be calculated given the temperature of the CMB. Then, if we know the effective number of relativistic degrees of freedom today,  $g_*(T_0)$ , we can compute  $h^2 \Omega_{\text{rad},0} = h^2 \Omega_\gamma / 2 \times g_*(T_0)$ , or apply Eq. (1) in Ref. [30].

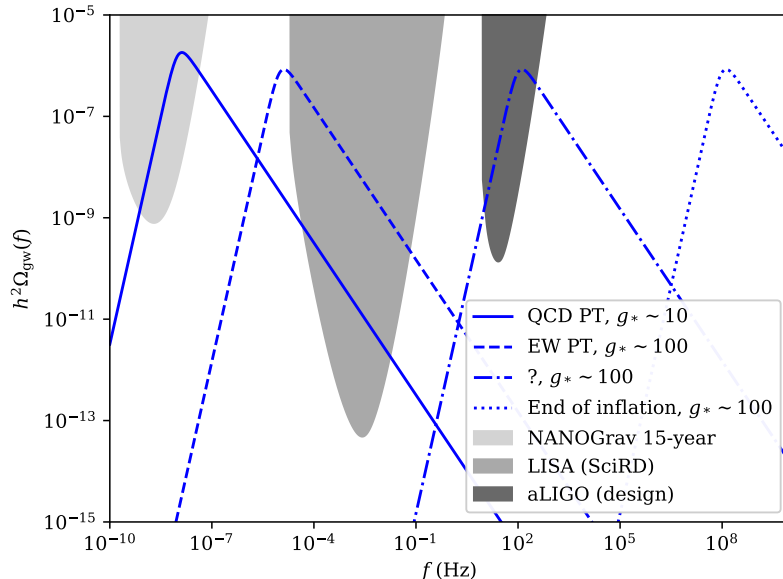


Figure 5: Best-case scenarios for gravitational wave power spectra, in the cases given in Table 1. Note that setting  $C = 0.1$  is a simplistic approach to computing the anticipated amplitude of the different scenarios, but that otherwise there is a very mild dependence on the number of relativistic degrees of freedom. Also shown are the power-law integrated sensitivity curves [32] anticipated for advanced LIGO and for LISA [33], each assuming a 5 year observation time, and for NANOGrav [34] based on the 15 year data release. If a background signal has a power-law shape and intersects the shaded regions, then in the absence of astrophysical foregrounds, it may be detectable. Our sensitivity curves assume a signal-to-noise ratio of 5.

the SNR comes from integrating the power spectrum over all frequencies, and also integrating over the time for which the detector will be sensitive to the source. The sensitivity curves in Figure 5 are so-called ‘power-law integrated sensitivity curves’, giving an indication of the typical amplitude of gravitational wave background that might be detectable.

The results of this section should apply to any process in the early universe that sourced gravitational waves on large scales. In the next section, we will discuss the physics of gravitational wave production after a first-order phase transition in particular.

### 3.4 Gravitational waves from a first order phase transition

We have seen already that a first-order phase transition involves bubbles of the new phase nucleating in space, expanding and merging together. We also pointed out that isolated spherical objects don’t source gravitational waves, because they don’t have any terms beyond the monopole when expanded in terms of spherical harmonics. The bubbles, as they expand, will generally create a reaction front in the plasma around them – if the particles which make up the plasma are coupled to the field undergoing the phase transition. The heated plasma inside the reaction front carries a lot of the energy released as latent heat during the transition, but we assume that this shell is also spherical.<sup>19</sup> On the other hand, if there is no such plasma, or it is only very weakly coupled to the field undergoing the phase transition, then the released energy goes into accelerating the bubble walls to ultrarelativistic speeds. We will return to this in Section 3.5.

The bubbles and associated reaction fronts continue to expand, and (if the universe is expanding slowly

<sup>19</sup>The hydrodynamical behaviour of this reaction front may be such that *instabilities* form, altering its shape away from an ideal sphere. However, this will happen on length scales many orders of magnitude shorter than the final bubble radius [35].



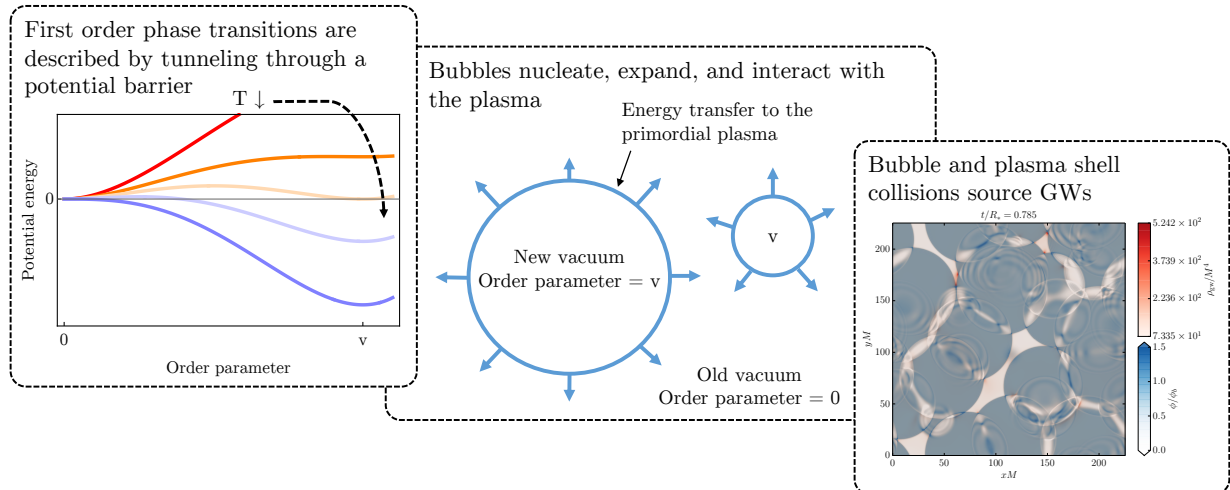


Figure 6: Illustration of the generation of gravitational waves in a first order phase transition. We thank Daniel Cutting for the simulation snapshot, based on work in Ref. [36].

enough) eventually collide with one another (see Fig. 6). At this point, the system starts to produce gravitational waves. The heated shells of plasma may (if the transition is not so strong) just pass through one another or (if the transition is stronger) interact nonlinearly with one another. If the heated plasma is mostly in front of the bubble wall (termed a deflagration), these interactions can raise the temperature and pressure and potentially slow the bubble wall down. Eventually, however, the bubbles will collide, leaving the whole universe in the new phase.

Both the colliding (and disappearing) scalar field bubbles and the overlapping shells of plasma are sources of gravitational waves. Even if the reaction fronts pass through each other without interacting strongly, they source gravitational waves through the stress-energy tensor for the plasma, which is proportional to fluid 4-velocity  $U^\mu$  squared:

$$T_{(f)}^{\mu\nu} = (e + p)U^\mu U^\nu, \quad (47)$$

where  $e$  is the energy and  $p$  the pressure in the plasma, and  $U^\mu$  is its four-velocity. This then forms the source on the right hand side of Eq. (15).

The general principle that led to Eq. (17) also applies to primordial gravitational waves – the system has to have a nonvanishing quadrupole moment in order to source gravitational waves. In practice, this happens when the bubbles and shells of plasma associated with them start to overlap. Note how the fluid velocity four-vector appears twice in Eq. (47). When the plasma shells overlap, the system cannot be decomposed into spherical shells with the same squared fluid velocity (see Fig. 7): the source is no longer spherically symmetric, the quadrupole moment is no longer zero, and gravitational waves are produced.

After the bubble walls have gone, the reaction fronts are free to move, and overlap with each other. Without a driving force provided by the latent heat of the transition, however, they propagate at the propagation speed for perturbations in a plasma: the speed of sound. Indeed, one can at this point think of the remnants of the reaction fronts as *shells of sound waves*. The shells can go on expanding, and overlapping with other shells, and sourcing gravitational waves—and, if the transition is strong enough, interacting nonlinearly with the other shells, too.

This goes on for a relatively long time, until either the universe expands enough for the energy in the sound waves to be attenuated, or nonlinearities in the plasma become significant. By dimensional analysis, this will happen on a timescale proportional to the most important length scale in the system divided by a typical velocity. Conventionally, this is taken to be the ratio of the bubble radius at collision  $R_*$  to the

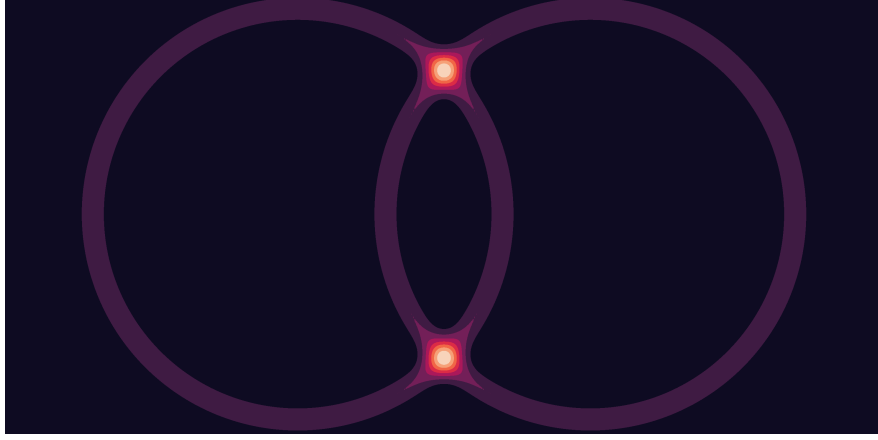


Figure 7: Illustration of the square of the 4-velocity for two overlapping plasma shells.

(enthalpy-weighted) root mean square 4-velocity  $\bar{U}_f$ ,

$$\tau_{\text{nl}} = \frac{R_*}{\bar{U}}. \quad (48)$$

This is typically called the *nonlinearity time* as the main thing which happens is the fluid field  $U^\mu$  develops nonlinearities on this scale. Notably, these will include discontinuities in the fluid termed *shocks* (in strong transitions, shocks can also be present at the leading or trailing edge of reaction fronts, but these will typically disappear after the transition). Other nonlinear behaviour, such as the establishment of turbulence, can also take place.

In most milder scenarios, however, the overlapping sound shells are the main source of gravitational waves. Based on computer simulations [37–39] (see Figure 6, right, for an example of a simulation configuration) an ansatz was developed for the gravitational wave power spectrum,

$$h^2 \Omega_{\text{sw}}(f) = 1.19 \times 10^{-6} \left( \frac{100}{g_*(T_*)} \right)^{\frac{1}{3}} \Gamma^2 \bar{U}_f^4 \left( \frac{H_*}{\beta} \right) v_w S_{\text{sw}}(f, f_0). \quad (49)$$

The spectral shape is similar to that mentioned in the previous section,

$$S_{\text{sw}}(f, f_0) = \left( \frac{f}{f_0} \right)^3 \left( \frac{7}{4 + 3(f/f_0)^2} \right)^{7/2} \quad (50)$$

where the peak frequency  $f_0$  is

$$f_0 = 8.9 \mu\text{Hz} \frac{1}{v_w} \left( \frac{\beta}{H_*} \right) \left( \frac{z_p}{10} \right) \left( \frac{T_*}{100 \text{ GeV}} \right) \left( \frac{g_*}{100} \right)^{\frac{1}{6}}. \quad (51)$$

Note that, in line with the general rules of thumb we developed above, the power goes as  $f^3$  at long wavelengths; and (51) is approximately Eq. 38 with the scale  $B$  set by  $R_*$ , the bubble radius at collision and assuming  $v_w \approx 1$ , and the factor  $z_p = 10$ . More subtle predictions are being developed, based on the assumption that the gravitational waves come entirely from overlapping sound shells – the ‘sound shell model’ [40, 41]. For example Refs. [42, 43] show that below the peak there is a wide ‘plateau’ with a relatively flat  $f^1$  power spectrum, before rising sharply to a peak with an  $f^9$  power law. These results have been validated by simulations.

In any case the above expression, (49), and the sound shell modelling results, are predicated on the assumption that  $\tau_{\text{nl}}$  in (48) is longer than the Hubble time  $1/H_*$ , so that the source is diluted by the expansion of the universe before nonlinearities start to matter. If that is not the case, then the ansätze above may no longer apply. How exactly they should be changed to produce accurate predictions in general remains an open research problem, but good progress is being made in understanding how the sound waves give rise to shocks and turbulence.

### 3.5 Vacuum and runaway transitions

Some scenarios, where the bubble wall moves very quickly, will not stir up enough kinetic energy in the plasma to create a lasting source of gravitational waves through sound waves. Some of these are so-called ‘runaway scenarios’, where there is friction between the bubble wall and the plasma, but it is insufficient to slow the wall down. Others arise when the field that forms the bubbles does not feel any plasma at all. In either case, the bubble walls accelerate to ultrarelativistic speeds.

Most of the potential energy released by the transition is converted into accelerating the bubble walls. The walls Lorentz contract at a rate which turns out to be proportional to the ratio of the bubble radius to its value at nucleation,  $R_0$

$$\gamma(R) = \frac{R}{R_0}. \quad (52)$$

This, in turn, means that scalar field gradient energy is stored in the walls. When the walls collide, a great deal of energy is released. Furthermore, with limited damping, the field which underwent the transition can continue to oscillate even after the bubbles have collided.

Because the walls get so Lorentz contracted, there is an even larger dynamic range required between the wall width and the bubble radius in order to get useful results from simulations, although there has been recent progress in matching the power spectrum to the underlying theory [36, 44].

Many attempts have been made to analyse these vacuum and runaway scenarios analytically. There is at the moment limited agreement between simulation and analytical models, however one of the most promising is the so-called ‘bulk flow model’ [45, 46].

## 4 Detection

Supposing, then, that one or more phase transitions did happen in the early universe, and they they did produce a cosmological stochastic background of gravitational waves. How would we go about detecting them? Or, conversely, if we understand the mechanisms of gravitational wave production sufficiently well, can we use gravitational waves to rule out certain theories or scenarios?

As we will show in this section, we will most likely need to go into space to detect a cosmological stochastic gravitational wave background, and missions like LISA will be our best chance. However, there are also indirect constraints on gravitational waves set by the cosmic microwave background and astrometric observations, as well as evidence for a gravitational wave background at nanoHertz frequencies seen by pulsar timing arrays.

### 4.1 Direct detection of gravitational waves

In 2015 the Laser Interferometer Gravitational-Wave Observatory detected a gravitational wave signal for the first time. Arising from the merger of two black holes at about 410 megaparsecs, this and subsequent discoveries have rekindled interest in direct detection of gravitational waves as a probe of cosmology and astrophysics.

The two detectors of LIGO, and other Earth-based missions including VIRGO and KAGRA, all function as very large, efficient Michelson interferometers.

#### 4.1.1 Detecting a gravitational wave with a Michelson interferometer

In a Michelson interferometer, a beam splitter sends coherent light down two perpendicular arms, at the end of which they are reflected by a mirror. When the light is recombined, the two split beams interfere (see Fig. 8). The interference can be constructive, or destructive, depending on the relative path lengths.

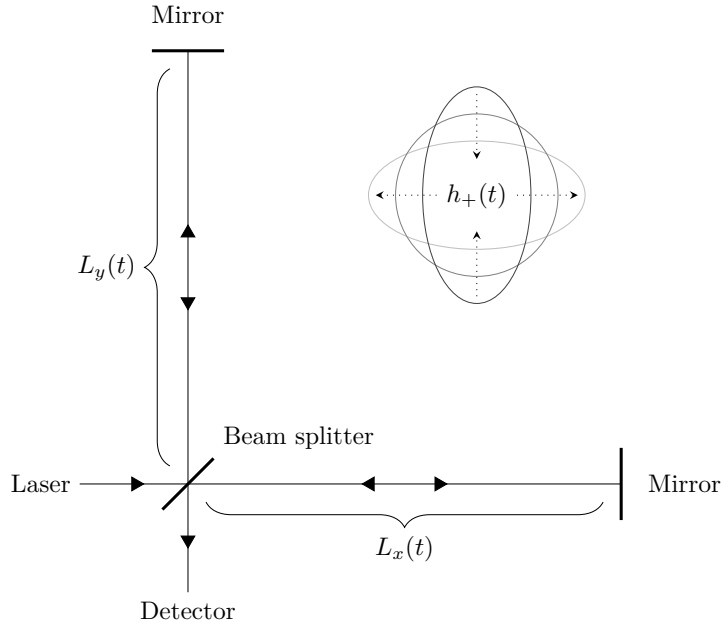


Figure 8: Schematic depiction of a Michelson interferometer for the detection of gravitational waves. The lengths  $L_x$  and  $L_y$  of the two interferometer arms can be thought of as time-varying, although a proper analysis requires computing the time taken for photons to travel from the beam splitter to each mirror and back again. The interferometers used by the LIGO/Virgo/KAGRA collaboration follow this general principle.

Following Ref. [24], let us suppose we build such an interferometer, and a gravitational wave passes through it perpendicular to the plane in which it lies. For simplicity, let us assume that the wave is fully polarised in the same directions as the arms:

$$h_{\times}(t) = 0; \quad h_{+}(t) = h_0 \cos(\omega_{\text{gw}} t) \quad (53)$$

where  $\omega_{\text{gw}}$  is the angular frequency of the gravitational wave and  $h_0$  is the strain amplitude. We will think of this as just a local stretching of spacetime and neglect all other gravitational effects on the detector.

We can then write down the metric, or infinitesimal interval,  $ds^2$ , noting that photons obey  $ds^2 = 0$ ,

$$ds^2 = c^2 dt^2 + [1 + h_{+}(t)] dx^2 + [1 - h_{-}(t)] dy^2 + dz^2. \quad (54)$$

We can use this to calculate the round-trip time for a photon down each arm, and thus the phase shift. Normally the Michelson interferometer is set up to destructively interfere when no gravitational waves are present, and so we are looking to get the largest signal out when our gravitational wave passes through. For a given angular frequency  $\omega_{\text{gw}}$ , this comes from requiring

$$\frac{\omega_{\text{gw}} L}{c} = \frac{\pi}{2} \Rightarrow L = \frac{\lambda_{\text{gw}}}{4}. \quad (55)$$

In other words, for gravitational waves around 100 Hz (such as those produced by stellar mass black hole binaries), we would need a 750 km detector. Luckily, advances in optics have meant that, by replacing the arms with Fabry-Pérot cavities, we can get this down to a few kilometres. On the other hand, if we want to detect gravitational waves with frequencies around 1 mHz, then something entirely different will be required.

#### 4.1.2 Time-delay interferometry in space

Space-based interferometer experiments such as the Laser Interferometry Space Antenna (LISA) and proposals such as DECIGO and TianQin are in many ways similar to their ground-based siblings. As on earth,

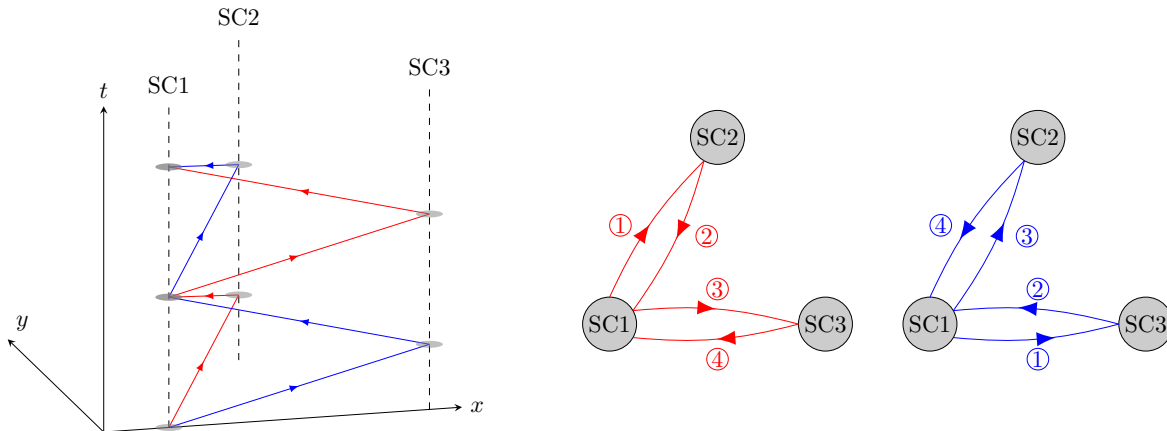


Figure 9: Schematic illustration of time delay interferometry, after Figure 2 in Ref. [48]. Three spacecraft (‘SC1’, ‘SC2’ and ‘SC3’) are depicted (at left) in some choice of reference frame, while (at right) two plan views of the three spacecraft show the order in which laser signals are combined to carry out measurements. Laser signals are sent from one spacecraft and then received by another, forming a one-way measurement. The simplest combinations that can be used to detect gravitational wave signals (a first-generation Michelson combination) is shown here: starting at SC1, one set of signals (red) involves measuring the delay to SC2 first and then SC3, while the other (blue) measures the delay to SC3 first and then SC1. These combinations can be thought of virtual laser beams, which interfere when they return to SC1. The combination of measured delays is not transmitted between spacecraft, it is instead constructed from the delay data afterwards.

these experiments take advantage of phase difference between laser beams to measure perturbations in the gravitational field. But space-based experiments can have much longer arms, and are therefore sensitive to much lower frequencies (and larger wavelengths). In the case of LISA, the arm-lengths will be approximately 2.5 million kilometres, such that the gravitational wave frequencies probed can be estimated using

$$f_{\text{gw}} = c/L = \frac{3.0 \times 10^5 \text{ km/s}}{2.5 \times 10^6 \text{ km}} = 0.12 \text{ Hz.} \quad (56)$$

In practice this is an overestimate; LISA is most sensitive around 3 mHz due to the anticipated noise sources and detector response.

Another difference is that it is impossible to maintain an equal distance between three spacecraft orbiting the sun, which means that the Michelson interferometer with one laser and two mirrors cannot be used. Furthermore, the constellation of the three spacecraft are rotating about the centroid of the triangle shape. The experiment could therefore naively be much more sensitive to laser noise with amplitudes far exceeding expected gravitational wave signals – by as many as ten orders of magnitude. The solution to this problem is time-delay interferometry [47]: if each of the spacecraft of a space-based interferometer can both receive and transmit laser signals, the laser noise from one transmitter can be measured by the others.

The laser noise of the receiving spacecraft enters the Doppler data immediately at the time of reception, while the laser noise of the transmitting spacecraft enters at a one-way delay time earlier. Because each spacecraft is transmitting laser light at the two other spacecraft, there are six such one-way measurements in the LISA constellation. Then, time-delayed combinations of these six signals can be compared to cancel out the laser noise while retaining gravitational wave signals (see Figure 9). In practice, these combinations can get quite elaborate, but are sufficient to bring the laser noise down to acceptable levels.

### 4.1.3 Atom interferometry

A different technique (see Ref. [49] for a recent accessible summary) to study low frequencies takes advantage of the fact that matter can behave like waves, especially at low temperatures. Particles such as atoms have

a deBroglie wavelength

$$\lambda_{\text{dB}} = \frac{h}{mv} \quad (57)$$

where  $h$  is Planck's constant. From this it is seen that the smaller the momenta of the particles (the lower their temperature), the longer the wavelength. In atom interferometers, ultra-cold atoms are accelerated using electromagnetic fields, split and brought back together to study the interference pattern just like in laser interferometry. When gravitational waves affect the travelling atoms, the interference pattern will be affected.

An important difference is that atoms are affected by the gravitational pull of the Earth much more than photons are. To account for this effect, atom interferometers usually have vertical beams in which the atoms are brought into free-fall. The frequency the experiments are sensitive to depends on the amount of time free-fall can be realised; in the 100 m shaft of the MAGIS-100 experiment for example, the atoms can be in free-fall for  $\sim 3$  s and therefore the sensitivity is  $f \sim 1/3$  Hz.

#### 4.1.4 Proposals to detect high frequency gravitational waves

Detecting high-frequency GWs is an active area of research in astrophysics and gravitational physics, aiming to open new windows into the universe beyond what has been possible with current low-frequency GW observatories like the ones described above. High-frequency gravitational waves, typically considered to be in the range of  $10^4$  Hz to  $10^9$  Hz, are challenging to detect with Michelson interferometers as the thermal and quantum noise in this frequency window is too large to make detections.

Various proposals are being explored to achieve this, including electromagnetic proposals primarily inspired by axion detectors (see e.g. [50]), resonant mass detectors that rely on the vibration of solid objects (see e.g. [51] for a review), and opto-mechanical devices that detect gravitational waves through changes in optical properties [52].<sup>20</sup> The direct detection of high frequency gravitational waves faces immense challenges, owing to the small wavelength and large noise. Accordingly, the sensitivity of these experimental proposals is not typically strong enough to detect early Universe gravitational wave backgrounds from before the electroweak epoch.

## 4.2 Indirect detection of gravitational waves

Besides the dedicated experiments measuring gravitational waves directly, their presence can also be inferred from a number of indirect probes. Vice versa, non-observation can be used to derive constraints.

### 4.2.1 Early universe probes

The polarisation of the photons comprising the CMB can be expressed in a basis of E-modes and B-modes. E-mode polarisation is in or perpendicular to the wave vector, B-mode polarisation is at a  $\pm 45^\circ$  angle. Density perturbations are a scalar quantity and only generate E-mode polarisation, but gravitational waves are tensors and generate both. B-modes have not been observed by CMB experiments such as Planck and BICEP2 [54, 55], which are sensitive to frequencies in the range  $10^{-20} - 10^{-16}$  Hz. Cosmic inflation itself leads to a gravitational wave spectrum which can be well approximated by a power-law  $\Omega_{\text{GW}} \propto (f/f_{\text{cmb}})^{n_t}$ , with a small negative spectral index  $n_t$  in the simplest models. Constraints are often reported in terms of the tensor-to-scalar ratio  $r = A_t/A_s$ , which measures the amplitude of the gravitational wave spectrum in terms of that of the scalar perturbations. The current constraint is  $r < 0.12$ , which corresponds to  $\Omega_{\text{GW}} \lesssim 10^{-14}$  at the pivot frequency  $f_{\text{cmb}} \sim 10^{-17}$  Hz. The next generation of CMB experiments, CMB stage-4, will improve upon this.

Any new form of energy in the universe contributes to its expansion rate, as captured by the Hubble constant. Non-relativistic or matter-like contributions are different from relativistic or radiation-like contributions, and

<sup>20</sup>For an extensive review on all proposals and further references, please refer to the living review [53].

both the CMB and measurements of the light elements produced in BBN can be used to determine quite how much relativistic energy there was during the BBN epoch. As gravitational wave energy is relativistic, this gives an upper bound on the total amount of gravitational waves produced in the early universe. This amount is often captured in terms of the effective number of neutrino species: i.e. how many neutrino-like particles there could be if they accounted for the radiation:

$$\frac{\Omega_{\text{GW},0}h^2}{\Omega_{\gamma,0}h^2} = \frac{1}{\Omega_{\gamma,0}h^2} \int d \log k \frac{1}{\rho_{\text{tot},0}} \frac{d\rho_{\text{GW},0}}{d \log k} = \frac{7}{8} \left( \frac{4}{11} \right)^{4/3} \Delta N_{\text{eff}}, \quad (58)$$

where the 0 denotes a present day quantity, and the present photon density is given by  $\Omega_{\gamma}h^2 = 2.47 \times 10^{-5}$ . At the moment, the limit is given by  $\Delta N_{\text{eff}} = N_{\text{eff}} - N_{\text{eff,SM}} \leq \mathcal{O}(10^{-1})$  [30], meaning that the integrated gravitational wave energy today is already constraint to be smaller than  $\mathcal{O}(10^{-7})$ . Next-generation experiments will push down further, to about  $\Delta N_{\text{eff}} \leq \mathcal{O}(10^{-2})$ , bringing the constraint down even more.

### 4.2.2 Pulsar timing arrays

Observations of the electromagnetic spectrum coming from astrophysical objects can also encode information about gravitational waves. Millisecond pulsars are an example. These rapidly spinning neutron stars have a period as stable as an atomic clock, and therefore serve as a sensitive probe of their environment. The presence of gravitational waves affects the pulses of EM radiation as they travel towards the Earth; careful monitoring of the pulse arrival times can therefore be used to detect or constrain gravitational waves. Pulsar timing arrays (PTAs) do just that; these dedicated experiments typically monitor a large number of pulsars weekly ( $\sim 10^{-6}$  Hz) and run for a number of years ( $\sim 10^{-8}$  Hz). This cadence is chosen primarily for the discovery of galactic binary mergers, in which galactic nuclei – supermassive black holes – play the most important role. But other signals, such as that generated by a first order phase transition at a relatively low scale could also fall within this frequency window. Currently, PTAs can probe microhertz gravitational waves with amplitude of about  $\Omega_{\text{GW}}(3\mu\text{ Hz})h^2 \leq 10^{-10}$  [56].

In 2020, the NANOGrav collaboration reported a signal that could be consistent with a stochastic gravitational wave background in the nanohertz range. This signal was observed in the timing residuals of an array of millisecond pulsars over a 12.5-year period. The detection was subsequently confirmed by other experiments: the European Pulsar Timing Array (EPTA), the Parkes Pulsar Timing Array (PPTA) in Australia, and the International Pulsar Timing Array (IPTA), which is a consortium of all these major groups. For a PTA signal to be confirmed as a gravitational wave background, and specifically as a signature of early universe phase transitions, subsequent data must reveal the Hellings-Downs correlation: this would show the characteristic quadrupolar spatial correlation. This indicates that the observed patterns are indeed due to the space-time ripples caused by gravitational waves, as opposed to any other confounding signals or noise. Evidence for this correlation was reported simultaneously in June 2023 by NANOGrav [57], the Chinese Pulsar Timing Array [58], EPTA and the Indian Pulsar Timing Array [59] and PPTA [60], with all of these results apparently in agreement with one another [61].

Since the PTA signal was reported, several studies have analysed the data. Some of these have found that early Universe signals such as first order phase transitions provide a better fit to the signal than supermassive black hole mergers (e.g. [62, 63]), based on basic modelling of both of these signals, though others showed inconclusive evidence or a preference for another source [64, 65]. Such a phase transition would have taken place at a temperature of the early Universe bath below the QCD scale (see Table 1 and Fig. 2), but above the scale of BBN ( $T \sim 2\text{ MeV}$ ), or otherwise light element abundances would be disrupted. A hidden sector, only gravitationally connected to the Standard Model, could have sourced the nanohertz GWs. Such a phase transition could also be supercooled, meaning that the universe remained in a metastable state longer than expected. This delay allows the bubbles of the new phase to grow larger and contain more energy, leading to stronger gravitational wave signals. The increased bubble size can also mean that the peak frequency of the emitted GWs is redshifted into the PTA-sensitive range.

A more definite answer on the source of the PTA signal may come from LISA, the space interferometer discussed in the previous section. Because LISA probes gravitational waves in a complementary frequency

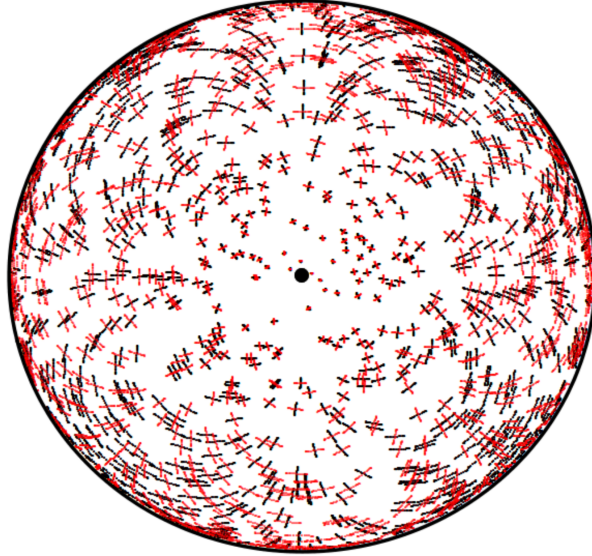


Figure 10: Demonstration of astrometry as a probe of gravitational waves. The image shows an orthographic projection of the Northern hemisphere with 103 stars, with a GW from the North pole (black dot) which causes the apparent position of stars to oscillate. The black (red) lines show movement tracks for a linearly plus (cross) polarisation. The GW amplitude has been exaggerated for clarity. Figure from [67], used with permission.

range, it can reveal more of the spectral shape of the signal, which can then be used to distinguish between the astrophysical and cosmological interpretations.

#### 4.2.3 Astrophysical probes

Precise astrometric observations of the motion of galactic stars can also be used to constrain gravitational waves. Galaxy surveys such as GAIA [66] make precise observations of  $\sim 10^9$  stars in our galaxy. Gravitational wave signals would interfere with the light of those stars as it travels towards the Earth, which would register as very small wiggles in their apparent position – see Fig. 10. Because statistical data analysis on the positions of  $10^9$  objects is computationally unfeasible, averages of sample averages can be taken without loss of sensitivity. Astrometric observations are sensitive to gravitational waves in a similar frequency range as PTAs, with similar sensitivity. This corresponds to distances of about a parsec in apparent shift:  $f_{\text{GW}} \sim c/1 \text{ pc} \sim 10^{-9} \text{ Hz}$ .

## 5 Conclusions and Outlook

The prospect of observing gravitational waves with millihertz frequencies serves as a strong motivation to study out-of-equilibrium dynamics in the very early universe. First order phase transitions – events which have been studied in connection with the matter/antimatter asymmetry, dark matter, and confinement – give rise to stochastic gravitational wave backgrounds. In this review we have discussed the particle physics behind a first order phase transition, how the subsequent dynamics gives rise to gravitational waves, and how the various experiments looking for gravitational waves work.

The particle physics models studied for their phase transitions can typically also be studied in other ways. For example, matter/antimatter asymmetry models which use the conditions of the electroweak phase transition usually also predict new particles at energy scales within reach of the next generation of particle colliders. Therefore, complimentary studies can inform gravitational wave searches, and vice versa: if a hint of new



physics is found in the gravitational wave data, follow up experiments will have to be done to verify more details of its nature.

For scientists interested in this research program, there is a lot of interesting work ahead. In the next two decades, many new experiments will start to produce data. To accurately find the implications of this data for particle physics, our techniques for calculating and modelling the phenomenology need to be improved. On the microphysics side, calculating the false vacuum decay rate and the subsequent expansion of critical bubbles suffers from theoretical uncertainty, related to finite temperature effects. On the computational side, studying the onset of turbulence in a relativistic plasma is a very big but important challenge.

**Acknowledgments:** D.C. is supported by the STFC under Grant No. ST/T001011/1. D.J.W. was supported by Research Council of Finland grant no. 324882.

## References

- [1] S. Staggs, J. Dunkley, and L. Page, Rept. Prog. Phys. **81**, 044901 (2018).
- [2] G. Aad *et al.* (ATLAS), Phys. Lett. B **716**, 1 (2012), arXiv:1207.7214 [hep-ex] .
- [3] S. Chatrchyan *et al.* (CMS), Phys. Lett. B **716**, 30 (2012), arXiv:1207.7235 [hep-ex] .
- [4] B. P. Abbott *et al.* (LIGO Scientific, Virgo), Phys. Rev. Lett. **116**, 061102 (2016), arXiv:1602.03837 [gr-qc] .
- [5] B. P. Abbott *et al.* (LIGO Scientific, Virgo), Phys. Rev. Lett. **119**, 161101 (2017), arXiv:1710.05832 [gr-qc] .
- [6] I. G. Moss, Contemp. Phys. **56**, 468 (2015), arXiv:1507.05760 [hep-ph] .
- [7] A. R. Liddle, in *ICTP Summer School in High-Energy Physics and Cosmology* (1999) pp. 260–295, arXiv:astro-ph/9901124 .
- [8] A. H. Guth, Phys. Rev. D **23**, 347 (1981).
- [9] A. Rajantie, Contemp. Phys. **53**, 195 (2012), arXiv:1204.3077 [hep-th] .
- [10] C. Quigg, Contemp. Phys. **48**, 1 (2007), arXiv:0704.2045 [hep-ph] .
- [11] P. Williams, Contemporary Physics **19**, 1 (1978).
- [12] P. A. Zyla *et al.* (Particle Data Group), PTEP **2020**, 083C01 (2020).
- [13] L. Husdal, Galaxies **4**, 78 (2016), arXiv:1609.04979 [astro-ph.CO] .
- [14] M. Maggiore, *Gravitational Waves. Vol. 2: Astrophysics and Cosmology* (Oxford University Press, 2018).
- [15] M. B. Hindmarsh, M. Lüben, J. Lumma, and M. Pauly, SciPost Phys. Lect. Notes **24**, 1 (2021), arXiv:2008.09136 [astro-ph.CO] .
- [16] T. Vachaspati, L. Pogosian, and D. Steer, Scholarpedia **10**, 31682 (2015), arXiv:1506.04039 [astro-ph.CO] .
- [17] S. R. Coleman, Phys. Rev. D **15**, 2929 (1977), [Erratum: Phys.Rev.D 16, 1248(E) (1977)].
- [18] C. G. Callan, Jr. and S. R. Coleman, Phys. Rev. D **16**, 1762 (1977).
- [19] A. Andreassen, D. Farhi, W. Frost, and M. D. Schwartz, Phys. Rev. Lett. **117**, 231601 (2016), arXiv:1602.01102 [hep-th] .

- [20] A. Andreassen, D. Farhi, W. Frost, and M. D. Schwartz, *Phys. Rev. D* **95**, 085011 (2017), arXiv:1604.06090 [hep-th] .
- [21] D. Croon, *PoS TASI2022*, 003 (2024), arXiv:2307.00068 [hep-ph] .
- [22] D. E. Morrissey and M. J. Ramsey-Musolf, *New J. Phys.* **14**, 125003 (2012), arXiv:1206.2942 [hep-ph] .
- [23] E. E. Flanagan and S. A. Hughes, *New J. Phys.* **7**, 204 (2005), arXiv:gr-qc/0501041 .
- [24] M. Maggiore, *Gravitational Waves. Vol. 1: Theory and Experiments*, Oxford Master Series in Physics (Oxford University Press, 2007).
- [25] A. Kosowsky, M. S. Turner, and R. Watkins, *Phys. Rev. D* **45**, 4514 (1992).
- [26] R. A. Isaacson, *Phys. Rev.* **166**, 1263 (1968).
- [27] R. A. Isaacson, *Phys. Rev.* **166**, 1272 (1968).
- [28] C. Caprini and D. G. Figueroa, *Class. Quant. Grav.* **35**, 163001 (2018), arXiv:1801.04268 [astro-ph.CO] .
- [29] S. Dodelson, *Modern Cosmology* (Academic Press, Amsterdam, 2003).
- [30] N. Aghanim *et al.* (Planck), *Astron. Astrophys.* **641**, A6 (2020), [Erratum: *Astron. Astrophys.* 652, C4 (2021)], arXiv:1807.06209 [astro-ph.CO] .
- [31] C. Caprini, R. Durrer, T. Konstandin, and G. Servant, *Phys. Rev. D* **79**, 083519 (2009), arXiv:0901.1661 [astro-ph.CO] .
- [32] E. Thrane and J. D. Romano, *Phys. Rev. D* **88**, 124032 (2013), arXiv:1310.5300 [astro-ph.IM] .
- [33] S. Babak, A. Petiteau, and M. Hewitson, (2021), arXiv:2108.01167 [astro-ph.IM] .
- [34] G. Agazie *et al.* (NANOGrav), *Astrophys. J. Lett.* **951**, L10 (2023), arXiv:2306.16218 [astro-ph.HE] .
- [35] A. Megevand and F. A. Membiela, *Phys. Rev. D* **89**, 103507 (2014), arXiv:1311.2453 [astro-ph.CO] .
- [36] D. Cutting, M. Hindmarsh, and D. J. Weir, *Phys. Rev. D* **97**, 123513 (2018), arXiv:1802.05712 [astro-ph.CO] .
- [37] M. Hindmarsh, S. J. Huber, K. Rummukainen, and D. J. Weir, *Phys. Rev. Lett.* **112**, 041301 (2014), arXiv:1304.2433 [hep-ph] .
- [38] M. Hindmarsh, S. J. Huber, K. Rummukainen, and D. J. Weir, *Phys. Rev. D* **92**, 123009 (2015), arXiv:1504.03291 [astro-ph.CO] .
- [39] M. Hindmarsh, S. J. Huber, K. Rummukainen, and D. J. Weir, *Phys. Rev. D* **96**, 103520 (2017), [Erratum: *Phys.Rev.D* 101, 089902 (2020)], arXiv:1704.05871 [astro-ph.CO] .
- [40] M. Hindmarsh, *Phys. Rev. Lett.* **120**, 071301 (2018), arXiv:1608.04735 [astro-ph.CO] .
- [41] M. Hindmarsh and M. Hijazi, *JCAP* **12**, 062 (2019), arXiv:1909.10040 [astro-ph.CO] .
- [42] R. Sharma, J. Dahl, A. Brandenburg, and M. Hindmarsh, *JCAP* **12**, 042 (2023), arXiv:2308.12916 [gr-qc] .
- [43] A. Roper Pol, S. Procacci, and C. Caprini, (2023), arXiv:2308.12943 [gr-qc] .
- [44] D. Cutting, E. G. Escartin, M. Hindmarsh, and D. J. Weir, *Phys. Rev. D* **103**, 023531 (2021), arXiv:2005.13537 [astro-ph.CO] .
- [45] T. Konstandin, *JCAP* **03**, 047 (2018), arXiv:1712.06869 [astro-ph.CO] .

- [46] R. Jinno, T. Konstandin, and M. Takimoto, *JCAP* **09**, 035 (2019), arXiv:1906.02588 [hep-ph] .
- [47] J. W. Armstrong, F. B. Estabrook, and M. Tinto, *ApJ* **527**, 814 (1999).
- [48] O. Hartwig, J.-B. Bayle, M. Staab, A. Hees, M. Lilley, and P. Wolf, *Phys. Rev. D* **105**, 122008 (2022), arXiv:2202.01124 [gr-qc] .
- [49] O. Buchmueller, J. Ellis, and U. Schneider, *Contemp. Phys.* **64**, 93 (2023), arXiv:2306.17726 [astro-ph.CO] .
- [50] V. Domcke, in *57th Rencontres de Moriond on Electroweak Interactions and Unified Theories* (2023) arXiv:2306.04496 [gr-qc] .
- [51] O. D. Aguiar, *Res. Astron. Astrophys.* **11**, 1 (2011), arXiv:1009.1138 [astro-ph.IM] .
- [52] A. Arvanitaki and A. A. Geraci, *Phys. Rev. Lett.* **110**, 071105 (2013), arXiv:1207.5320 [gr-qc] .
- [53] N. Aggarwal *et al.*, *Living Rev. Rel.* **24**, 4 (2021), arXiv:2011.12414 [gr-qc] .
- [54] P. A. R. Ade *et al.* (BICEP2, Planck), *Phys. Rev. Lett.* **114**, 101301 (2015), arXiv:1502.00612 [astro-ph.CO] .
- [55] Y. Akrami *et al.* (Planck), *Astron. Astrophys.* **641**, A10 (2020), arXiv:1807.06211 [astro-ph.CO] .
- [56] Z. Arzoumanian *et al.* (NANOGrav), *Astrophys. J. Lett.* **905**, L34 (2020), arXiv:2009.04496 [astro-ph.HE] .
- [57] G. Agazie *et al.* (NANOGrav), *Astrophys. J. Lett.* **951**, L8 (2023), arXiv:2306.16213 [astro-ph.HE] .
- [58] H. Xu *et al.*, *Res. Astron. Astrophys.* **23**, 075024 (2023), arXiv:2306.16216 [astro-ph.HE] .
- [59] J. Antoniadis *et al.* (EPTA, InPTA:), *Astron. Astrophys.* **678**, A50 (2023), arXiv:2306.16214 [astro-ph.HE] .
- [60] D. J. Reardon *et al.*, *Astrophys. J. Lett.* **951**, L6 (2023), arXiv:2306.16215 [astro-ph.HE] .
- [61] G. Agazie *et al.* (International Pulsar Timing Array), *Astrophys. J.* **966**, 105 (2024), arXiv:2309.00693 [astro-ph.HE] .
- [62] J. Ellis, M. Fairbairn, G. Franciolini, G. Hütsi, A. Iovino, M. Lewicki, M. Raidal, J. Urrutia, V. Vaskonen, and H. Veermäe, *Phys. Rev. D* **109**, 023522 (2024), arXiv:2308.08546 [astro-ph.CO] .
- [63] Y.-M. Wu, Z.-C. Chen, and Q.-G. Huang, *Sci. China Phys. Mech. Astron.* **67**, 240412 (2024), arXiv:2307.03141 [astro-ph.CO] .
- [64] D. G. Figueroa, M. Pieroni, A. Ricciardone, and P. Simakachorn, *Phys. Rev. Lett.* **132**, 171002 (2024), arXiv:2307.02399 [astro-ph.CO] .
- [65] L. Bian, S. Ge, J. Shu, B. Wang, X.-Y. Yang, and J. Zong, *Phys. Rev. D* **109**, L101301 (2024), arXiv:2307.02376 [astro-ph.HE] .
- [66] T. Prusti *et al.* (Gaia), *Astron. Astrophys.* **595**, A1 (2016), arXiv:1609.04153 [astro-ph.IM] .
- [67] C. J. Moore, D. P. Mihaylov, A. Lasenby, and G. Gilmore, *Phys. Rev. Lett.* **119**, 261102 (2017), arXiv:1707.06239 [astro-ph.IM] .